



Enhanced corrosion resistance of micro-arc oxidation coated magnesium alloy by superhydrophobic Mg–Al layered double hydroxide coating

Zhi-hu WANG¹, Ju-mei ZHANG², Yan LI¹, Li-jing BAI¹, Guo-jun ZHANG¹

1. School of Materials Science and Engineering, Xi'an University of Technology, Xi'an 710048, China;
2. School of Materials Science and Engineering, Xi'an University of Science and Technology, Xi'an 710054, China

Received 4 January 2019; accepted 29 May 2019

Abstract: To further enhance the corrosion resistance of the porous micro-arc oxidation (MAO) ceramic layers on AZ31 magnesium alloy, superhydrophobic Mg–Al layered double hydroxide (LDH) coating was fabricated on MAO-coated AZ31 alloy by using in-situ growth method followed by surface modification with stearic acid. The characteristics of different coatings were investigated by XRD, SEM and EDS. The effect of the hydrothermal treatment time on the formation of the LDH coatings was studied. The results demonstrated that the micro-pores and cracks of MAO coating were gradually sealed via in-situ growing LDH with prolonging hydrothermal treating time. Electrochemical measurement displayed that the lowest corrosion current density, the most positive corrosion potential and the highest impedance modulus were observed for superhydrophobic LDH/MAO coating compared with those of MAO coating and LDH/MAO coating. Immersion experiment proved that the superhydrophobic LDH/MAO coating with the active anti-corrosion capability significantly enhanced the long-term corrosion protection for MAO coated alloy.

Key words: magnesium alloy; micro-arc oxidation; layered double hydroxide; superhydrophobicity; corrosion resistance

1 Introduction

Micro-arc oxidation (MAO), also referred to as plasma electrolytic oxidation (PEO), is an electrochemical surface treatment process developed from conventional anodic oxidation [1]. As an industrial technology for surface protection, the MAO treatment has been successfully used to form the ceramic film on the surface of magnesium alloy, which main aims to improve the corrosion resistance [2–6]. Nevertheless, some research results show that MAO ceramic films consist of an inner thin compact layer and an outer thick porous layer, and the unavoidable micro-pores and micro-cracks on the surface forming during the MAO process reduced the corrosion resistance of the substrate, because corrosive solution could easily infiltrate into the substrate through these defects and lead to the degradation and failure of the protective coating [7,8]. Meanwhile, DING et al [9] believed that the presence of second phase Mg₂Ca in Mg–1Li–1Ca alloy played an important role in the formation of MAO coating and the

MAO coating began to degrade from intermetallic compound Mg₂Ca.

In order to enhance the protective properties of the MAO coating, it would be of great significance to remedy the surface defects of the MAO coating. Thus, sealing treatments for blocking the pores and cracks can play an important role in enhancing the protection against corrosion [10]. In addition, it is a remarkable fact that the micro-pores and micro-cracks of the MAO coatings can provide mechanical interlocking sites, which can significantly improve the long-lasting adhesion between the coating prepared subsequently and the MAO film [1,11].

Layered double hydroxide (LDH), with a brucite-like lamellar structure, is made up of positively charged sheets and interlayer region containing charge-balancing anions and water molecules [12]. LDH, owing to its interesting properties in compositional flexibility and anion-exchange capacity, has already been applied to a “smart” self-healing coating to protect the metal materials [13]. To today, in-situ growth technique using hydrothermal treatment and anion-exchange is the main

Foundation item: Project (17JS083) supported by the Key Laboratory Program of Shaanxi Education Department, China; Project (2016JZ018) supported by the Key Program of Natural Science Research of Shaanxi Province, China; Project (51701162) supported by the National Natural Science Foundation of China

Corresponding author: Guo-jun ZHANG; Tel: +86-29-82312592; E-mail: zhangguojun@xaut.edu.cn
DOI: 10.1016/S1003-6326(19)65113-7

method to prepare LDH coating on the surface of magnesium alloy [14–20]. Of course, there are other methods to prepare LDH film on magnesium alloy surface, such as electrochemical deposition [21], spinning coating [22] and steam coating [23].

Table 1 lists the thickness and corrosion current density (J_{corr}) of different LDH coatings on magnesium alloy from most recent published literatures. The conclusion can be drawn from Table 1 that the J_{corr} of LDH film directly fabricated on the surface of magnesium alloy could be reduced by 1–2 orders of magnitude compared with bare magnesium alloy and the corrosion resistance was enhanced to some extent. However, these results are still not suitable for the use of magnesium alloys in harsh environments. Recently, the preparation of LDH coatings on the surface of anodization or micro-arc oxidation coated on magnesium alloys has been reported [24–26]. Their results illustrated that the loose and porous oxide films were completely sealed by LDH nanosheets, and the corrosion resistance was significantly enhanced, where J_{corr} could be reduced by 2–3 orders of magnitude compared with uncoated magnesium alloy. However, the porous and hydrophilic outer layer of LDH provides infiltration channels or spaces to accommodate the corrosive medium, increasing the possibility of coating deterioration, and the failure of the coating [16,27]. Due to the layered structure with high porosity and roughness, LDH films are easy to get superhydrophobic properties by chemical modification with low surface free energy materials which could contribute to the anti-corrosion [27,28].

Therefore, taking these advantages into consideration, it is extremely significant to enhance the corrosion resistance of magnesium alloy by sealing the pores and cracks of the MAO coating and obtaining superhydrophobic surface. In this work, the Mg–Al LDH coating was fabricated on the surface of MAO coated AZ31 magnesium alloy using the simple hydrothermal treatment. Subsequently, the LDH/MAO composite coating was modified with long-chain stearic acid and

the superhydrophobic surface was obtained. The structure and morphology of different coatings were characterized by X-ray diffractometer (XRD), scanning electronic microscope (SEM) and energy dispersive spectrometer (EDS), and the corrosion behavior of the coatings was characterized by means of electrochemical measurement and immersing test.

2 Experimental

2.1 Specimens preparation

MAO coating was prepared on the AZ31 Mg alloy (the nominal compositions in wt.%: 2.5–3.5 Al, 0.6–1.3 Zn, 0.1 Si, 0.04 Ca, 0.2–0.8 Mn, 0.05 Cu and balanced Mg) with a constant voltage of 360 V at 600 Hz for 480 s using 1 kW AC power supply with a duty cycle of 10%. Prior to MAO treatment, the samples were cut into 20 mm × 20 mm × 4 mm and mechanically ground with SiC paper, ultrasonically cleaned in ethyl alcohol, and then dried in cold air. The electrolyte of alkaline silicate was composed of 20 g/L $\text{Na}_2\text{SiO}_3 \cdot 9\text{H}_2\text{O}$, 10 g/L NaOH and a small amount of $\text{KF} \cdot 2\text{H}_2\text{O}$.

A hydrothermal treatment was used to fabricate Mg–Al LDH on the MAO coating. The hydrothermal solution consisted of 0.05 mol/L $\text{Al}(\text{NO}_3)_3 \cdot 9\text{H}_2\text{O}$ and the pH (10.5) was adjusted by diluted ammonia. The MAO coated sample was placed into Teflon-lined autoclaves and completely submerged into the transferred solution above. Then, the autoclaves were tightened and put into drying oven at 125 °C for 6, 12, 18 and 24 h, respectively. After hydrothermal treatment, obtained samples were denoted as LDH-6 h/MAO, LDH-12 h/MAO, LDH-18 h/MAO, and LDH-24 h/MAO, respectively. To achieve surface superhydrophobicity, the LDH-24 h/MAO sample was immersed in an ethanol solution with 0.05 mol/L stearic acid for 5 h at 60 °C. Finally, the modified sample was rinsed with ethanol three times and then dried in air, and the obtained sample was denoted as SA-LDH-24 h/MAO.

Table 1 Thickness and corrosion current density of different LDH coatings on magnesium alloy from most recent published literature

Substrate	LDH coating	Corrosive medium	Thickness/ μm	J_{corr} (Substrate)/($\text{A} \cdot \text{cm}^{-2}$)	J_{corr} (LDH coating)/($\text{A} \cdot \text{cm}^{-2}$)	Ref.
AZ91D	Mg–Al– CO_3^{2-}	3.5 wt.% NaCl	5–8	2×10^{-4}	$< 1.2 \times 10^{-4}$	[14]
AZ31	Mg–Al– CO_3^{2-}	3.5 wt.% NaCl	7	3.04×10^{-5}	6.52×10^{-8}	[15]
AZ31	Mg–Al– MoO_4^{2-}	3.5 wt.% NaCl	17	3.17×10^{-5}	1.6×10^{-7}	[16]
AZ91D	Zn–Al– NO_3^-	3.5 wt.% NaCl	–	6.42×10^{-4}	1.33×10^{-5}	[17]
AZ91D	Zn–Al– Cl^-	3.5 wt.% NaCl	4.7	6.42×10^{-4}	2.52×10^{-6}	[17]
AZ91D	Zn–Al– VO_x^-	3.5 wt.% NaCl	5.2	6.42×10^{-4}	2.21×10^{-6}	[17]
AZ31	Mg–Al– CO_3^{2-}	3.5 wt.% NaCl	25–50	3.37×10^{-5}	5.75×10^{-6}	[18]
AZ31D	Mg–Al– CO_3^{2-}	3.5 wt.% NaCl	20	5.264×10^{-6}	1.467×10^{-6}	[19]
JDBM	Mg–Al– CO_3^{2-}	3.5 wt.% NaCl	2.6	1.56×10^{-5}	3.63×10^{-7}	[20]

2.2 Characterization

The phase structures of different coatings as well as AZ31 substrate were examined using X-ray diffractometer (XRD, XRD-7000, Japan). The morphologies and chemical composition of the coating samples were characterized before and after immersion by field emission scanning electronic microscope (SEM, Merlin Compact, Germany) equipped with an energy dispersive X-ray spectrometer (EDS, Oxford Instruments, Britain). The surface wettability of coated samples was evaluated by measuring the water contact angles at room temperature using an optical contact angle measuring instrument (SDC-200, China).

2.3 Evaluation of corrosion resistance

The corrosion resistance of the specimens was evaluated in 3.5 wt.% NaCl solution at room temperature through an electrochemical corrosion test. An electrochemical workstation (PARSTAT, 4000, USA) and a typical three-electrode cell were used for electrochemical measurements. The saturated calomel electrode (SCE) was used as the reference electrode, uncoated and coated AZ31 Mg alloy sample (exposed area, 1 cm²) as the working electrode and the platinum electrode as the counter electrode. Before measurement, the working electrode was immersed in the quiescent test solution until the cell open circuit potential (OCP) became stable. The polarization curve was subsequently measured from -500 to +500 mV of OCP with a scanning rate of 2 mV/s. The electrochemical parameters such as the corrosion potential (ϕ_{corr}), corrosion current density (J_{corr}), and Tafel slope (β_c , β_a) were all derived from the polarization curves by Tafel extrapolation using electrochemical software. At the same time, the polarization resistance (R_p) was estimated with the Stein–Geary equation [7,28]:

$$R_p = \frac{\beta_a \cdot \beta_c}{2.303 J_{\text{corr}} (\beta_a + \beta_c)} \quad (1)$$

The electrochemical impedance spectroscopy (EIS) measurements were carried out in the frequency range of 10⁻¹–10⁵ Hz using a 5 mV amplitude perturbation. The obtained EIS plot was analyzed and fitted using Zview software.

In order to determine the long-term corrosion resistance of the coating, a total immersion test was carried out in 3.5 wt.% NaCl solution. The MAO coating, LDH-24 h/MAO coating and SA-LDH-24 h/MAO coating were subjected to the immersion test. Each sample was placed in a beaker with 40 mL NaCl solution, and then the beaker was sealed with plastic wrap and stood at room temperature. The immersion time lasted for 288 h and the NaCl solution was replaced by fresh one once three days.

3 Results and discussion

3.1 Coating characterization

XRD patterns of AZ31 substrate, MAO coated sample before and after hydrothermal treatment with different time are shown in Fig. 1. Only the diffraction peaks of Mg were detected in the pattern of uncoated AZ31 magnesium alloy, and the XRD pattern of the sample after MAO treatment depicts that the sample surface is mainly composed of mixed oxides of Mg and Al (MgO and MgAl₂O₄) and a small amount of Mg₂SiO₄ phases [29]. The existence of Mg₂SiO₄ phase in the MAO coating further confirms that the silicate ions in the electrolyte participate in the reaction to form the ceramic layer [4,28]. It is worth noting that no XRD peaks were observed in the 2 θ range between 5° and 20° in the case of uncoated and MAO coated sample; however, the diffraction peaks at 11.72° appeared corresponding to the characteristic reflections of (003) after hydrothermal reaction, suggesting the formation of Mg–Al LDH [26]. Furthermore, the diffraction intensity of LDH became stronger with the prolonging of the hydrothermal treatment time.

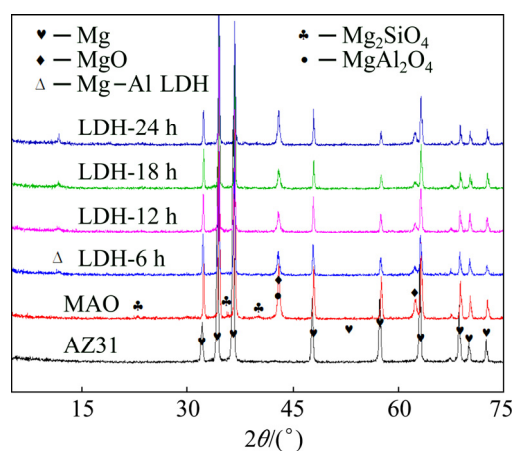


Fig. 1 XRD patterns of AZ31 substrate and coated samples

The SEM morphologies and EDS analysis results of the MAO coating before and after hydrothermal treatment with different time are presented in Fig. 2. The as-prepared MAO coating exhibited a typical porous morphology with micro-cracks and micro-pores, which would make the surface of the treated Mg alloy appear to be coarse and rough (Fig. 2(a)). The formation of micro-pores was mainly ascribed to the sparking discharge, gas bubble and the considerably low Pilling Bedworth (PB) ratio of Mg oxide to Mg substrate [7]. It can be noteworthy that these porous characteristics of MAO coating are gradually changed along with the increase of the hydrothermal treatment time. For the LDH-6 h/MAO sample, the porosity of the film was

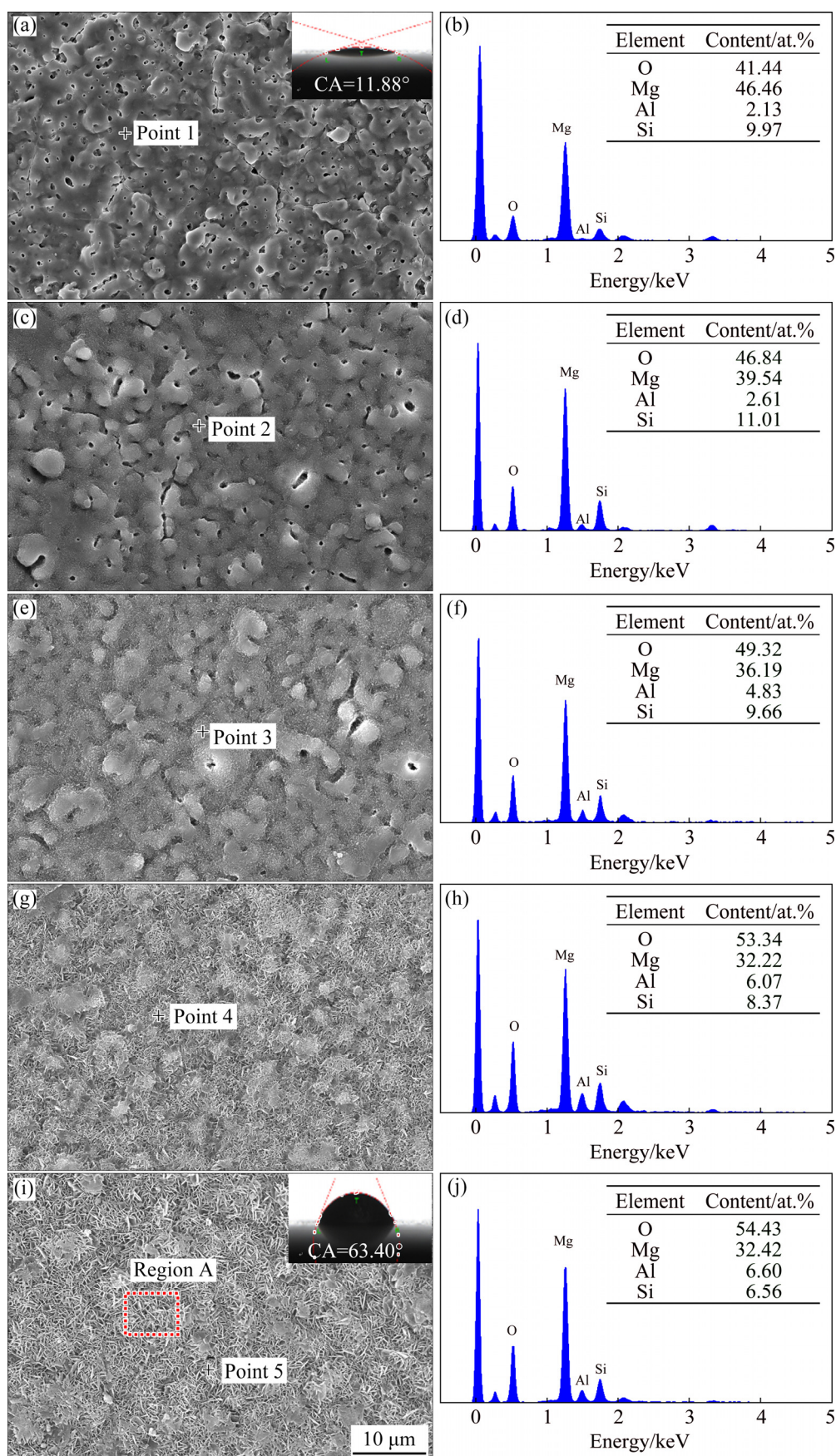


Fig. 2 SEM morphologies (a, c, e, g, i), contact angle (inset) and EDS analysis results (b, d, f, h, j) of MAO (a, b), LDH-6 h/MAO (c, d), LDH-12 h/MAO (e, f), LDH-18 h/MAO (g, h) and LDH-24 h/MAO (i, j) coatings

reduced but micro-pores and micro-cracks still existed, as shown in Fig. 2(c). When the hydrothermal treatment time increased to 12 h, the porosity of the film was significantly reduced. There were only a few holes on the surface of LDH-12 h/MAO sample, and the surface of film became smoother. However, with further prolonging processing time to 18 and 24 h, many nest-like and flake-like clusters presented on the surface of the MAO coating, and micro-pores and micro-cracks of the MAO coating were completely covered by hydrothermal product, as can be seen from Figs. 2(g, i). In addition, EDS results showed that the MAO and LDH/MAO sample were mainly composed of Mg, O, Al and Si elements. But the element contents of the LDH/MAO coating were different from those of MAO coating, indicating that Al^{3+} in the solution took part in the formation of Mg–Al LDH coating during the hydrothermal treatment. Moreover, the content of aluminum on the surface of LDH/MAO composite coating increased gradually with increasing treatment time. As can be seen from inset in Fig. 2(a), the porous

MAO coating showed hydrophilic behavior with a contact angle of 11.88° . After hydrothermal treatment for 24 h, the inherent defect of the porous oxide coating was covered with LDH nanosheets, resulting in a highly compact composite coating with a contact angle of 63.40° , as shown in Fig. 2(i), which was still hydrophilic.

The SEM surface morphology at higher magnification in Region A of Fig. 2(i) is shown in Fig. 3(a), and the electronic image as well as corresponding elemental mapping images are shown in Figs. 3(b–f). Figure 3(a) shows that the LDH nanosheets grew vertically from the surface of MAO coated AZ31 alloy, with a typical flake-like structure. As shown in Figs. 3(c–f), Mg, O, Al and Si elements uniformly distributed on the surface of sample with LDH/MAO coating. Among them, Mg and O elements mainly came from mixed oxides of Mg and Al produced in the MAO treatment, while Si and Al elements primarily originated from the electrolyte of MAO and hydrothermal solution, respectively. The uniform distribution of elements

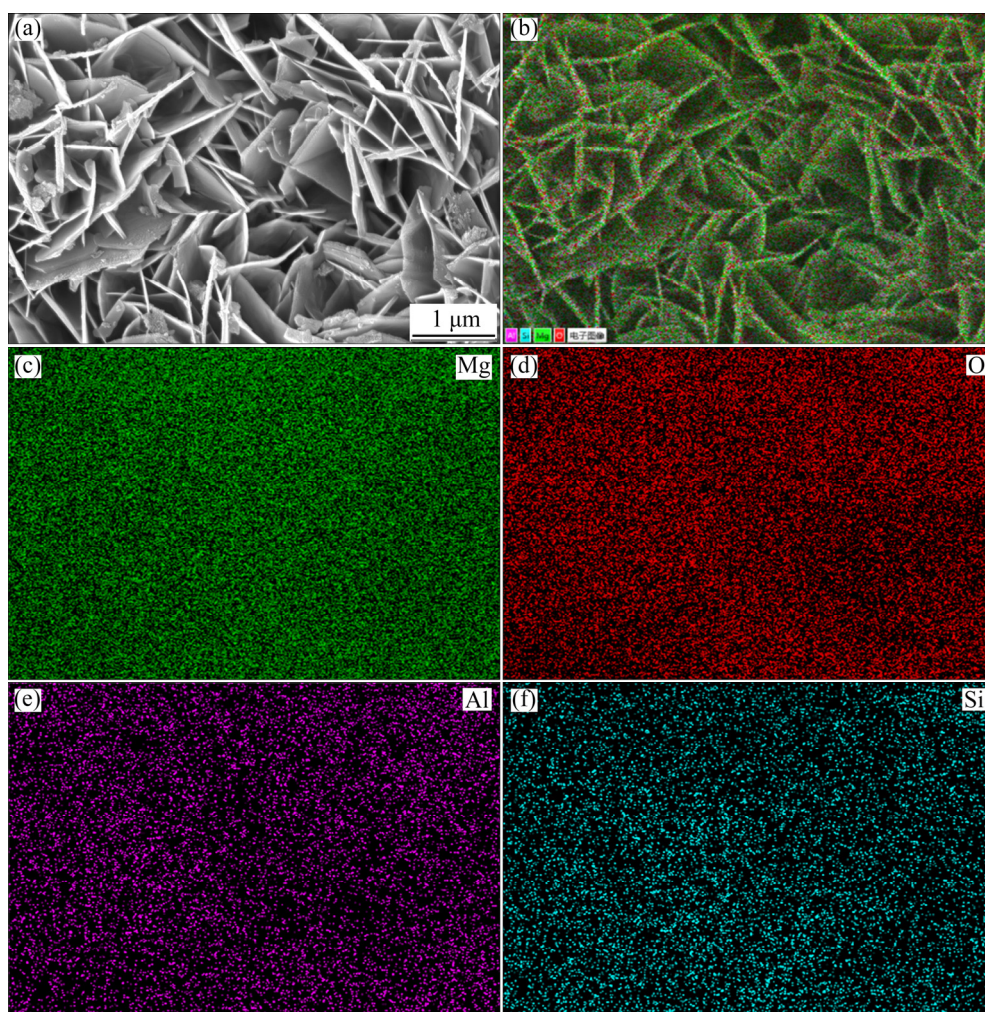


Fig. 3 SEM morphology (a) in Region A of Fig. 2(i), electronic image (b) and EDS elemental mapping images (c–f) of LDH-24 h/MAO coating

demonstrated that Mg and Si ions derived from partially dissolving of MAO ceramic coating were involved in the fabrication of LDH.

The cross-sectional SEM morphology and the line scanning images of LDH-24 h/MAO coating are shown in Fig. 4. According to the line scanning images, the thickness of the LDH-24 h/MAO composite coating was approximately 8.62 μm . It can be seen that the MAO ceramic layer grew on the substrate with good adhesion after the MAO treatment, and the LDH coating was strongly adhered to MAO coating after the hydrothermal treatment. It is worthy of noting that the interface between the MAO and LDH coating was not apparent, indicating that the LDH nanosheets grew from micro-pores and micro-cracks and covered the whole surface.

Figures 5(a) and (b) show the surface morphologies of the LDH-24 h/MAO coating after modification with

stearic acid at lower and higher magnifications. Compared with the original surface morphology of the LDH-24 h/MAO coating shown in Fig. 3(a), the surface structure was denser and had fewer pores, and most nanosheets were tiled on the surface after surface modification with stearic acid. However, as can be seen from inset in Fig. 5(b), the superhydrophobic property of the LDH/MAO composite coating was observed after surface modification, and its contact angle was 151.21°. The EDS data, as shown in Fig. 5(c), showed that the surface of the superhydrophobic composite coating contained Mg, O, Si and Al elements, and element contents had almost no significant difference compared with LDH-24 h/MAO coating (shown in Fig. 2(j)). Meanwhile, structure of as-prepared LDH-24 h/MAO coating before and after modification were characterized using XRD, as shown in Fig. 5(d). Apparently, no new

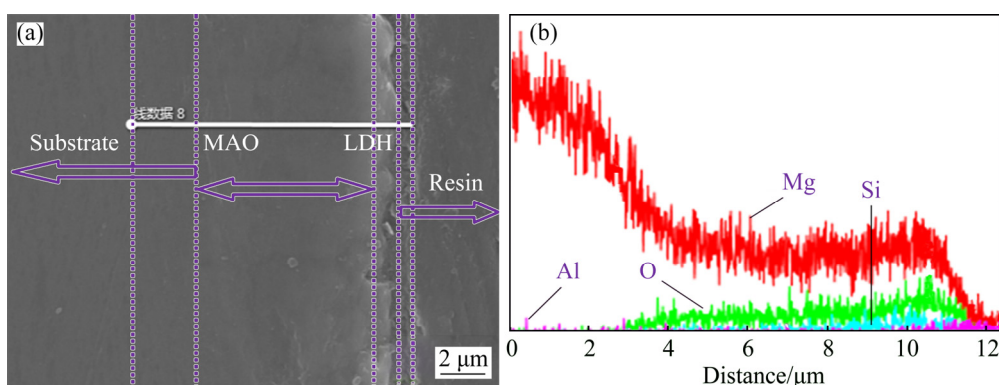


Fig. 4 Cross-sectional morphology (a) and line scanning mapping (b) of LDH-24 h/MAO coating

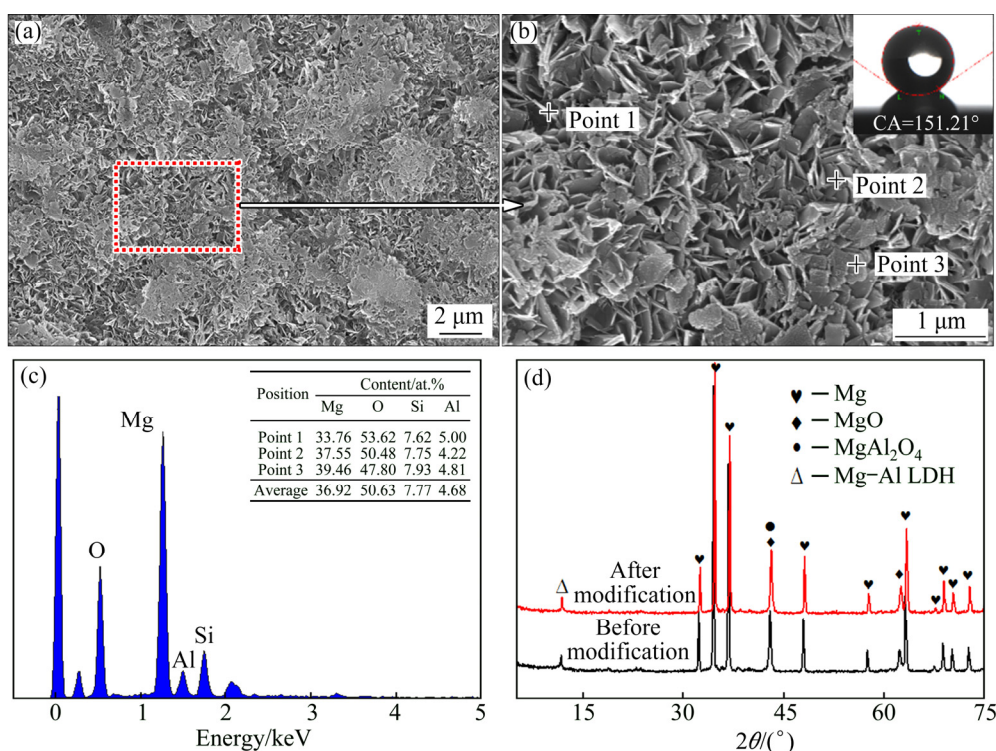


Fig. 5 SEM morphologies (a, b), contact angle (inset in Fig. 5(b)), EDS analysis result (c), and XRD patterns (d) of LDH-24 h/MAO coating after modification with stearic acid

phase appeared on the XRD pattern of the superhydrophobic composite coating, indicating that the phase did not change after modification. Nevertheless, the carboxyl group of stearic acid reacted with the hydroxyl group on the surface of LDH during the immersion, which was then grafted on the surface of the sample by means of chemical bond, reducing the surface energy of the sample. So, the superhydrophobic behavior after surface modification was attributed to the synergistic effect of the microstructure of the LDH coating and the low surface energy of stearic acid.

3.2 Corrosion resistance of coatings

The polarization curves of AZ31 substrate, MAO coating, LDH-24 h/MAO coating and superhydrophobic composite coating after being immersed in 3.5 wt.% NaCl solution for 30 min are presented in Fig. 6 and the corresponding corrosion parameters are listed in Table 2. Compared with uncoated AZ31 substrate, all the coated samples showed significant lower corrosion current density (J_{corr}) and more positive corrosion potential (ϕ_{corr}). In addition, the polarization resistance (R_p) of coated samples was obviously higher than that of uncoated AZ31 substrate. Based upon the experimental results of the polarization measurement, the superhydrophobic

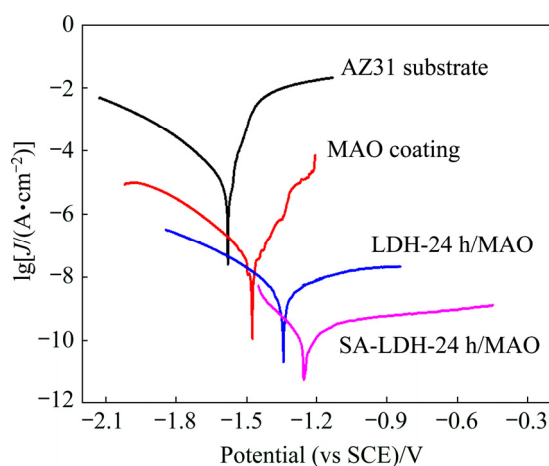


Fig. 6 Polarization curves of AZ31 substrate and coated samples

Table 2 Fitting results of polarization curves of AZ31 substrate and coated samples

Sample	ϕ_{corr}/V	$J_{\text{corr}}/(\text{A}\cdot\text{cm}^{-2})$	β_a/V	β_c/V	$R_p/(\Omega\cdot\text{cm}^2)$
AZ31 substrate	-1.5794	1.20×10^{-5}	0.185	0.152	3.02×10^3
MAO coating	-1.4742	4.31×10^{-8}	0.936	0.206	1.70×10^6
LDH-24 h/MAO	-1.3431	4.67×10^{-9}	0.562	0.235	1.54×10^7
SA-LDH-24 h/MAO	-1.2572	1.78×10^{-10}	0.897	0.143	3.01×10^8

composite coating possessed the most positive ϕ_{corr} , the lowest J_{corr} and the highest R_p compared with MAO coating and LDH-24 h/MAO composite coating, indicating that the corrosion resistance of the AZ31 substrate was effectively enhanced by this superhydrophobic composite coating.

In order to further evaluate the corrosion behavior of different coated samples, EIS measurement was carried out in NaCl solution at open circuit potential. Figure 7 presents the test results and fitting lines of Nyquist and Bode plots for uncoated AZ31 substrate and three different coatings. Different equivalent circuits, as shown in Fig. 8, were used to fit EIS for the uncoated sample and coated samples and the fitting results are listed in Table 3. As can be seen from Fig. 7(a), the Nyquist plot of uncoated Mg alloy consisted of a capacitive loop at high frequency and an inductive loop at low frequency. The equivalent circuit of the AZ31 substrate for fitting is shown in Fig. 8(a), where R_s , R_{ct} and CPE represent solution resistance, charge transfer resistance and constant phase element, respectively. CPE is defined by Y_0 and n . If n is equal to 1, CPE is identical to a capacitor [30]. In addition, R_L is a resistor at low frequency, ascribed to the appearance of pitting and peeling-off of the corrosion products, and L is the inductance [5,11,17,30]. The equivalent circuit of the coated sample is shown in Fig. 8(b). For MAO coating, the CPE_{out} and R_{out} represent the capacitance and resistance of the porous layer of MAO coating, respectively, and CPE_{inn} and R_{inn} represent the capacitance and resistance of the dense inside of MAO coating, respectively [30–32]. For the LDH/MAO compound coatings, CPE_{out} and R_{out} represent the capacitance and resistance of the outer LDH layer, respectively, and CPE_{inn} and R_{inn} represent the capacitance and resistance of the inner layer of MAO coating sealed by LDH nanosheets, respectively [17,24,25]. For the superhydrophobic LDH/MAO compound coatings, CPE_{out} and R_{out} represent the capacitance and resistance of the outer layer of compound coating, respectively, and CPE_{inn} and R_{inn} represent the capacitance and resistance of the inner layer of compound coating, respectively [33].

It is known that coatings on the metal substrates with a higher impedance modulus at lower frequency ($|Z|_{f=0.1\text{ Hz}}$) and larger radius of the capacitive loop exhibit a better corrosion resistance [25,34]. It can be seen that the fitted curves of the Nyquist plots for each sample are mainly composed of capacitive loop. As can be seen from Fig. 7(a), the dimension of the capacitive loop of uncoated AZ31 substrate was very small, suggesting that the corrosion resistance of uncoated AZ31 substrate is very poor. And it is obvious that the dimension of the capacitive loop was greatly increased for the AZ31 alloy

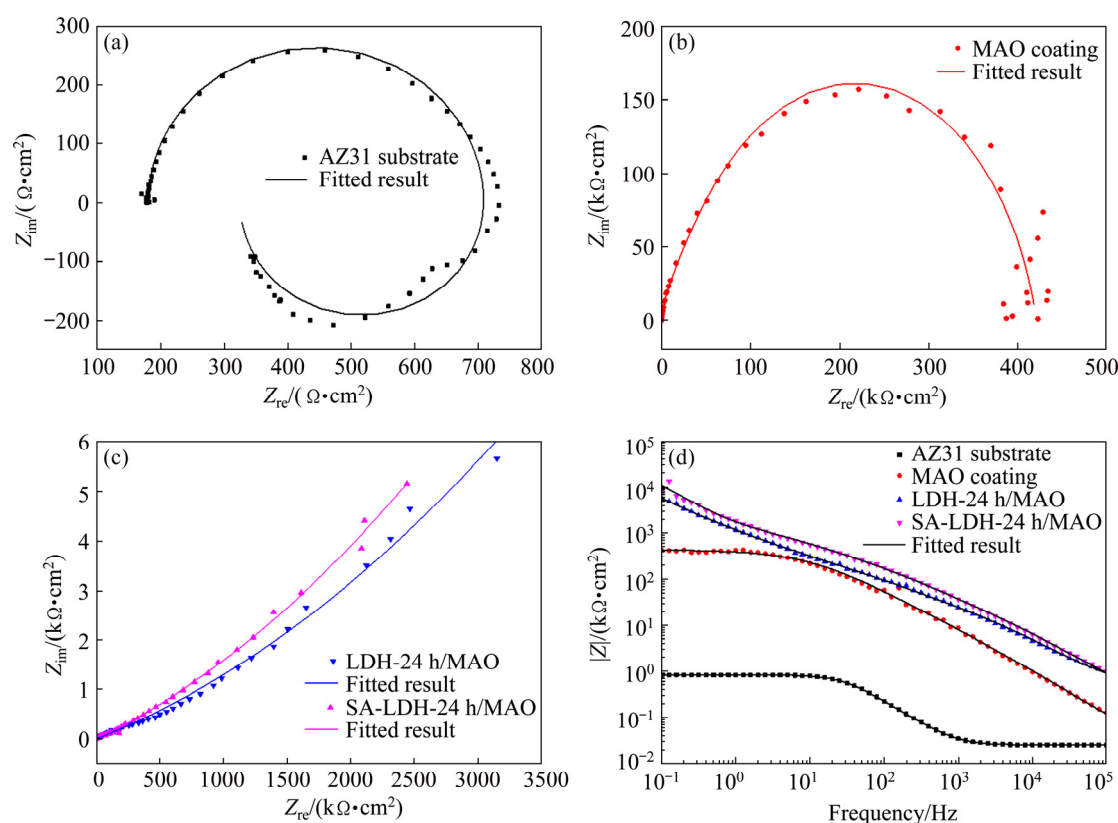


Fig. 7 EIS plots and equivalent circuits of AZ31 substrate and different coatings: (a–c) Nyquist plots; (d) Bode plot

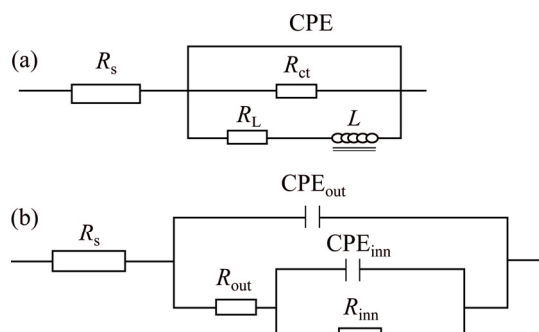


Fig. 8 Equivalent circuits used to fit EIS plots for uncoated Mg alloy (a) and coated Mg alloy (b)

with the MAO coating, as shown in Fig. 7(b). Although there were many micro-pores on the surface of the MAO coating, the micro-pores were not interconnected and the inner ceramic layer was compact, so the MAO coating can provide corrosion protection for AZ31 alloy. However, for the LDH-24 h/MAO coating and superhydrophobic composite coating, the diameter of the capacitive loop was much larger than that of the AZ31 substrate, as shown in Fig. 7(c). Especially, the Nyquist plot of the LDH-24 h/MAO sample after modification possessed the largest radius of curvature, which indicated that the superhydrophobic composite coating could lead to a higher corrosion resistance. This was because the micro-pores of the MAO layer were completely sealed

by LDH nanosheets and the water-repelling of the composite coating surface was improved after modification, which prevented corrosive media from infiltrating and reaching the coating surface. It could be seen from the Bode plots shown in Fig. 7(d) that the coated samples exhibited higher impedance at low frequency compared to the uncoated AZ31 substrate. Note also that the $|Z|_{f=0.1 \text{ Hz}}$ of the MAO coating was $4.33 \times 10^5 \Omega \cdot \text{cm}^2$, considerably higher than that of the substrate, which was $826 \Omega \cdot \text{cm}^2$. Furthermore, it was worth noting that the $|Z|_{f=0.1 \text{ Hz}}$ of the LDH-24 h/MAO composite coating was larger than that of the MAO coated sample, which was $5.70 \times 10^6 \Omega \cdot \text{cm}^2$. Especially, the $|Z|_{f=0.1 \text{ Hz}}$ of the superhydrophobic composite coating was the largest among the three coating coated samples, which was $1.09 \times 10^7 \Omega \cdot \text{cm}^2$. The EIS test results indicated that LDH-24 h/MAO coating after modification possessed the largest dimension of the capacitive loop and the highest impedance at low frequency, suggesting that the superhydrophobic composite coating had an excellent anti-corrosion effect. From the fitting data shown in Table 3, LDH-24 h/MAO coating had higher values of R_{out} and R_{inn} , compared with the MAO coating. The R_{out} and R_{inn} of the superhydrophobic composite coating were of the same order of magnitude compared to the LDH-24 h/MAO coating, but the R_{out} and R_{inn} were the highest. The reason for

increasing of R_{out} and R_{inn} could be the sealing effect and the inner MAO layer with more compact structure as well as the superhydrophobicity of the composite coating surface. The EIS results were in good accordance with the results from the polarization curves in Fig. 6.

3.3 Protection ability of coatings

Figure 9 presents the surface morphologies at low and higher magnifications and EDS analysis results of different coated samples after immersion in 3.5 wt.% NaCl solution for 288 h at room temperature. As can be seen from Figs. 9(a, b), the MAO coating showed severe corrosion damage after 288 h immersion compared to the original surface of MAO coating shown in Fig. 2(a). It is obvious that many corrosion products and micro-cracks distributed on the surface. When the MAO coated sample was immersed in the NaCl solution, the Cl^- ion in the solution could easily get through the micro-pores of the MAO coating and reached the interface between coating

and substrate, and then corrosion occurred. As shown in Fig. 9(c), MAO coating was mainly composed of O, Mg, Al and Si elements after immersion, and the reason for the presence of Na and Cl elements should be the adsorption of NaCl crystals on the surface. The formation of micro-cracks could be attributed to the extrusion stress induced by the accumulation of corrosion products $Mg(OH)_2$ [35,36].

However, the porous MAO ceramic layer sealed by LDH had an obvious difference in comparison with the MAO coating after 288 h of immersion. As can be seen from Fig. 9(d), most areas of samples still exhibited a flake-like morphology, and only few “corrosion pits” were observed. However, from the higher magnification SEM image, as shown in Fig. 9(e), there was no corrosion product in and around the “corrosion pit”, and the LDH with flake-like structure still existed at the bottom of the “corrosion pits”, which suggested that a part of LDH nanosheets on the surface of composite

Table 3 Main fitted parameters of EIS plots for uncoated and coated samples

Sample	$R_s/$ ($\Omega \cdot \text{cm}^2$)	$Y_0/$ ($\Omega^{-1} \cdot \text{cm}^{-2} \cdot \text{s}^{-n}$)	n	$R_{ct}/$ ($\Omega \cdot \text{cm}^2$)	$R_L/$ ($\Omega \cdot \text{cm}^2$)	$L/$ ($\text{H} \cdot \text{cm}^2$)	$R_{out}/$ ($\Omega \cdot \text{cm}^2$)	$Y_0'/$ ($\Omega^{-1} \cdot \text{cm}^{-2} \cdot \text{s}^{-n'}$)	n'	$R_{inn}/$ ($\Omega \cdot \text{cm}^2$)
AZ31 substrate	25.09	7.841×10^{-6}	0.98	692.6	111.8	194.5	—	—	—	—
MAO coating	20.98	4.069×10^{-8}	0.92	—	—	—	9.199×10^4	8.665×10^{-8}	0.80	3.239×10^5
LDH-24 h/MAO	32.53	4.426×10^{-8}	0.77	—	—	—	1.485×10^5	1.738×10^{-7}	0.67	6.968×10^6
SA-LDH-24 h/MAO	75.34	3.044×10^{-8}	0.77	—	—	—	5.795×10^5	1.170×10^{-7}	0.73	9.372×10^7

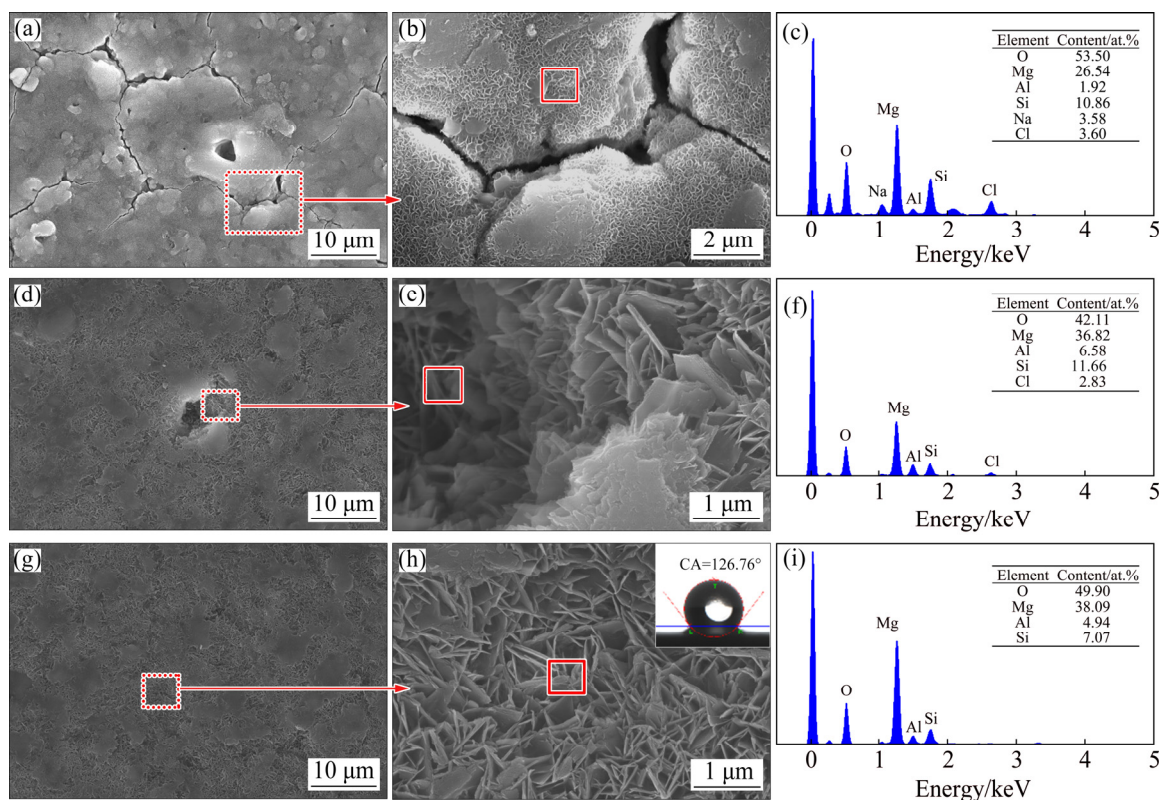


Fig. 9 Surface morphologies (a, b, d, e, g, h) and EDS analysis results (c, f, i) of MAO coating (a, b, c), LDH-24 h/MAO (d, e, f) and SA-LDH-24 h/MAO (g, h, i) after immersion in 3.5 wt.% NaCl solution for 288 h at room temperature

coating began to dissolve when the soak time reached 288 h. According to EDS energy spectrum shown in Fig. 9(f), the surface composition of the sample with LDH/MAO coating after soaking contained Cl element, indicating that LDH coating possessed ion-exchange capacity by capturing Cl^- from NaCl solutions and storing them in the interlayer of the LDH [25,34]. The above results showed that the anti-corrosion of the MAO ceramic coating could be further improved by preparing LDH coating on the surface of the MAO layer. It was noteworthy that the surface morphology (Figs. 9(g, h)) and EDS analysis results (Fig. 9(i)) of the superhydrophobic composite coating after immersion were almost the same as those before immersion, but the edges of LDH nanosheets were more distinct. Moreover, as could be seen in the inset from Fig. 9(h), the contact angle of LDH/MAO composite coating modified by stearic acid was 126.76° after immersion. This also indicated that the superhydrophobic coating had good stability in the process of soaking for 288 h. The superhydrophobic composite coating on the surface of the sample could resist the invasion of chloride ions and significantly improved the corrosion resistance of the alloy. The immersion test results were in good accordance with the results from the polarization curves and EIS analysis.

4 Conclusions

(1) Mg–Al LDH coating was fabricated on MAO coated AZ31 magnesium alloy by a facile in-situ growth method. The micro-pores and micro-cracks of MAO coating were gradually sealed via in-situ growing Mg–Al LDH with prolonging of hydrothermal treatment duration.

(2) The surface of Mg–Al LDH/MAO composite coating was modified by stearic acid, and the superhydrophobic surface with the best sealing effect was successfully constructed.

(3) Electrochemical and immersion experiments proved that the corrosion resistance of different coating ranked as follows: SA-LDH-24 h/MAO > LDH-24 h/MAO > MAO coating. MAO coating only provided a passive corrosion protection, while the superhydrophobic LDH/MAO composite coating provided an active corrosion protection for magnesium substrate.

(4) The reason of the excellent corrosion resistance of the superhydrophobic LDH/MAO composite coating can be attributed to the synergistic effect of the water repellency of the surface, the ability of the LDH coating to capture and store chlorine ions and the barrier effect of the sealed MAO coating.

References

- [1] SANKARA NARAYANAN T S N, PARK II S, LEE M H. Strategies to improve the corrosion resistance of microarc oxidation (MAO) coated magnesium alloys for degradable implants: Prospects and challenges [J]. *Progress in Materials Science*, 2014, 60: 1–71.
- [2] WANG Shu-yan, SI Nai-chao, XIA Yong-ping, LIU Li. Influence of nano-SiC on microstructure and property of MAO coating formed on AZ91D magnesium alloy [J]. *Transactions of Nonferrous Metals Society of China*, 2015, 25: 1926–1934.
- [3] DONG Chen, WANG Rui-qiang, HUANG Zhi-quan, WU Ye-kang, ZHANG Yi, WU Guo-rui, LI Da-long, GUO Chang-hong, JIANG Gui-rong, YU Sheng-xue, SHEN De-jiu, NASH P. Evolution processes of the corrosion behavior and structural characteristics of plasma electrolytic oxidation coatings on AZ31 magnesium alloy [J]. *Applied Surface Science*, 2018, 434: 326–335.
- [4] PEZZATO L, ANGELINI V, BRUNELLI K, MARTINI C, DABALÀ M. Tribological and corrosion behavior of PEO coatings with graphite nanoparticles on AZ91 and AZ80 magnesium alloys [J]. *Transactions of Nonferrous Metals Society of China*, 2018, 28: 259–272.
- [5] CUI Xue-jun, YANG Rui-song, LIU Chun-hai, YU Zu-xiao, LIN Xiu-zhou. Structure and corrosion resistance of modified micro-arc oxidation coating on AZ31B magnesium alloy [J]. *Transactions of Nonferrous Metals Society of China*, 2016, 26: 814–821.
- [6] CUI Lan-yue, LIU Han-peng, XUE Kui, ZHANG Wen-le, ZENG Rong-chang, LI Shuo-qi, XU Dao-kui, HAN En-hou, GUAN Shao-kang. In vitro corrosion and antibacterial performance of micro-arc oxidation coating on AZ31 magnesium alloy: Effects of tannic acid [J]. *Journal of the Electrochemical Society*, 2018, 165: C821–C829.
- [7] DUAN Hong-ping, DU Ke-qin, YAN Chuan-wei, WANG Fu-hui. Electrochemical corrosion behavior of composite coatings of sealed MAO film on magnesium alloy AZ91D [J]. *Electrochimica Acta*, 2006, 51: 2898–2908.
- [8] DONG Kai-hui, SONG Ying-wei, SHAN Da-yong, HAN En-hou. Formation mechanism of a self-sealing pore micro-arc oxidation film on AM60 magnesium alloy [J]. *Corrosion Science*, 2015, 100: 275–283.
- [9] DING Zi-You, CUI Lan-Yue, CHEN Xiao-Bo, ZENG Rong-chang, GUAN Shao-kang, LI Shuo-qi, ZHANG Fen, ZOU Yu-hong, LIU Qing-yun. In vitro corrosion of micro-arc oxidation coating on Mg–1Li–1Ca alloy—The influence of intermetallic compound Mg₂Ca [J]. *Journal of Alloys and Compounds*, 2018, 764: 250–260.
- [10] CUI Lan-yue, GAO Shang-dong, LI Ping-ping, ZENG Rong-chang, ZHANG Fen, LI Shuo-qi, HAN En-hou. Corrosion resistance of a self-healing micro-arc oxidation/polymethyltrimethoxysilane composite coating on magnesium alloy AZ31 [J]. *Corrosion Science*, 2017, 118: 84–95.
- [11] ZHANG Chang-lei, ZHANG Fen, SONG Liang, ZENG Rong-chang, LI Shuo-qi, HAN En-hou. Corrosion resistance of a superhydrophobic surface on micro-arc oxidation coated Mg–Li–Ca alloy [J]. *Journal of Alloys and Compounds*, 2017, 728: 815–826.
- [12] GUO Lian, WU Wei, ZHOU Yong-feng, ZHANG Fen, ZENG Rong-chang, ZENG Jian-min. Layered double hydroxide coatings on magnesium alloys: A review [J]. *Journal of Materials Science and Technology*, 2018, 34: 1455–1466.

- [13] TEDIM J, KUZNETSOVA A, SALAK A N, MONTEMOR F, SNIHIROVA D, PILZ M, ZHELUDKEVICH M L, FERREIRA M G S. Zn–Al layered double hydroxides as chloride nanotraps in active protective coatings [J]. *Corrosion Science*, 2012, 55: 1–4.
- [14] LIN J K, UAN J Y. Formation of Mg, Al-hydroxide conversion coating on Mg alloy in aqueous $\text{HCO}_3^-/\text{CO}_3^{2-}$ and corresponding protection against corrosion by the coating [J]. *Corrosion Science*, 2009, 51: 1181–1188.
- [15] ZHANG Fen, LIU Zhen-guo, ZENG Rong-chang, LI Shuo-qi, CUI Hong-zhi, SONG Liang, HAN En-hou. Corrosion resistance of Mg–Al–LDH coating on magnesium alloy AZ31 [J]. *Surface and Coatings Technology*, 2014, 258: 1152–1158.
- [16] ZENG Rong-chang, LIU Zhen-guo, ZHANG Fen, LI Shuo-qi, CUI Hong-zhi, HAN En-hou. Corrosion of molybdate intercalated hydroxide conversion coating on AZ31 Mg alloy [J]. *Journal of Materials Chemistry A*, 2014, 2: 13049–13057.
- [17] ZHOU Meng, YAN Lu-chun, LING Hao, DIAO Yu-peng, PANG Xiao-lu, WANG Yan-lin, GAO Ke-wei. Design and fabrication of enhanced corrosion resistance Zn–Al layered double hydroxides films based anion-exchange mechanism on magnesium alloys [J]. *Applied Surface Science*, 2017, 404: 246–253.
- [18] ZENG Rong-chang, LIU Zhen-guo, ZHANG Fen, LI Shuo-qi, HE Qing-kun, CUI Hong-zhi, HAN En-hou. Corrosion resistance of in-situ Mg–Al hydroxide conversion film on AZ31 magnesium alloy by one-step formation [J]. *Transactions of Nonferrous Metals Society of China*, 2015, 25: 1917–1925.
- [19] WANG Jun, LI Dan-dan, YU Xiang, JING Xiao-yan, ZHANG Mi-lin, JIANG Zhao-hua. Hydroxide conversion coating on Mg alloy and its corrosion resistance [J]. *Journal of Alloys and Compounds*, 2010, 494: 271–274.
- [20] PENG Feng, LI Hua, WANG Dong-hui, TIAN Peng, YUAN Guang-yin, XU De-min, LIU Xuan-yong. Enhanced corrosion resistance and biocompatibility of magnesium alloy by Mg–Al-layered double hydroxide [J]. *ACS Applied Materials and Interfaces*, 2016, 8: 35033–35044.
- [21] SYU J H, UAN J Y, LIN Meng-chang, LIN Zhi-yu. Optically transparent Li–Al–CO₃ layered double hydroxide thin films on an AZ31 Mg alloy formed by electrochemical deposition and their corrosion resistance in a dilute chloride environment [J]. *Corrosion Science*, 2013, 68: 238–248.
- [22] ZHANG Fa-zhi, SUN Ming, XU Sai-long, ZHAO Li-li, ZHANG Bo-wen. Fabrication of oriented layered double hydroxide films by spin coating and their use in corrosion protection [J]. *Chemical Engineering Journal*, 2008, 141: 362–367.
- [23] KAMIYAMA N, PANOMSUWAN G, YAMAMOTO E, SUDARE T, SAITO N, ISHIZAKI T. Effect of treatment time in the Mg(OH)₂/Mg–Al LDH composite film formed on Mg alloy AZ31 by steam coating on the corrosion resistance [J]. *Surface and Coatings Technology*, 2016, 286: 172–177.
- [24] ZHANG Gen, WU Liang, TANG Ai-tao, CHEN Xiao-bo, MA Yan-long, LONG Ying, PENG Peng, DING Xing-xing, PAN Hui-ling, PAN Fu-sheng. Growth behavior of MgAl-layered double hydroxide films by conversion of anodic films on magnesium alloy AZ31 and their corrosion protection [J]. *Applied Surface Science*, 2018, 456: 419–429.
- [25] WU Liang, YANG Dan-ni, ZHANG Gen, ZHANG Zhi, ZHANG Sheng, TANG Ai-tao, PAN Fu-sheng. Fabrication and characterization of Mg–M layered double hydroxide films on anodized magnesium alloy AZ31 [J]. *Applied Surface Science*, 2017, 431: 177–186.
- [26] PENG Feng, WANG Dong-hui, TIAN Ya-xin, CAO Hui-liang, QIAO Yu-qin, LIU Xuan-yong. Sealing the pores of PEO coating with Mg–Al layered double hydroxide: Enhanced corrosion resistance, cytocompatibility and drug delivery ability [J]. *Scientific Reports*, 2017, 7: 8167.
- [27] ZHANG Fen, ZHANG Chang-lei, ZENG Rong-chang, SONG Liang, GUO Lian, HUANG Xiao-wen. Corrosion resistance of the superhydrophobic Mg(OH)₂/Mg–Al layered double hydroxide coatings on magnesium alloys [J]. *Metals*, 2016, 85: 1–14.
- [28] ZHOU Meng, PANG Xiao-lu, WEI Liang, GAO Ke-wei. In-situ grown superhydrophobic Zn–Al layered double hydroxides films on magnesium alloy to improve corrosion properties [J]. *Applied Surface Science*, 2015, 337: 172–177.
- [29] DAROONPARVAR M, YAJID M A M, GUPTA R K, YUSOF N M, BAKHSHESHI-RAD H R, GHANDVAR H, GHASEMI E. Antibacterial activities and corrosion behavior of novel PEO/nanostructured ZrO₂ coating on Mg alloy [J]. *Transactions of Nonferrous Metals Society of China*, 2018, 28: 1571–1581.
- [30] YAO Zhong-ping, XIA Qi-xing, CHANG Li-ming, LI Chao-nan, JIANG Zhao-hua. Structure and properties of compound coatings on Mg alloys by micro-arc oxidation/hydrothermal treatment [J]. *Journal of Alloys and Compounds*, 2015, 633: 435–442.
- [31] LUO Dan, LIU Yan, YIN Xiao-ming, WANG Hui-yuan, HAN Zhi-wu, REN Lu-quan. Corrosion inhibition of hydrophobic coatings fabricated by micro-arc oxidation on an extruded Mg–5Sn–1Zn alloy substrate [J]. *Journal of Alloys and Compounds*, 2018, 731: 731–738.
- [32] ZHAN Xiao-qiang, SHANG Wei, WEN Yu-qing, LI Yu-qing, MA Ming-ming. Preparation and corrosion resistance of a three-layer composite coating on the Mg alloy [J]. *Journal of Alloys and Compounds*, 2019, 774: 522–531.
- [33] ZHANG Gen, TANG Ai-tao, WU Liang, ZHANG Ze-yu, LIAO Hong-xin, LI-Ling-jie, ATRENS A, PAN Fu-sheng. In-situ grown super- or hydrophobic Mg–Al layered double hydroxides films on the anodized magnesium alloy to improve corrosion properties [J]. *Surface and Coatings Technology*, 2019, 366: 238–247.
- [34] ZHANG Gen, WU Liang, TANG Ai-tao, MA Yan-long, SONG Guang-lin, ZHENG Da-jiang, JIANG Bin, ATRENS A, PAN Fu-sheng. Active corrosion protection by a smart coating based on a MgAl-layered double hydroxide on a cerium-modified plasma electrolytic oxidation coating on Mg alloy AZ31 [J]. *Corrosion Science*, 2018, 139: 370–382.
- [35] ZHANG Gen, WU Liang, TANG Ai-tao, ZHANG Shuo, YUAN Bo, ZENG Zhi-cheng, PAN Fu-sheng. A novel approach to fabricate protective layered double hydroxide films on the surface of anodized Mg–Al alloy [J]. *Advanced Materials Interfaces*, 2017, 4: 1700163.
- [36] SONG Guang-ling, SHI Zhi-ming. Corrosion mechanism and evaluation of anodized magnesium alloys [J]. *Corrosion Science*, 2014, 85: 126–140.

镁合金微弧氧化陶瓷层表面超疏水 Mg–Al 层状双金属氢氧化物涂层的耐蚀性

王志虎¹, 张菊梅², 李妍¹, 白力静¹, 张国君¹

1. 西安理工大学 材料科学与工程学院, 西安 710048;
2. 西安科技大学 材料科学与工程学院, 西安 710054

摘要: 为进一步提高镁合金微弧氧化多孔陶瓷层的耐蚀性, 采用原位水热法及硬脂酸表面改性方法, 在陶瓷层表面制备超疏水镁铝层状双金属氢氧化物(Mg–Al LDH)涂层。采用 X 射线衍射仪、扫描电子显微镜及能谱仪研究涂层的结构、形貌及成分, 研究水热处理时间对 Mg–Al LDH 膜形成的影响。结果表明, 随着水热处理时间的延长, 原位生长的 Mg–Al LDH 将 MAO 陶瓷层表面的微孔和微裂纹逐渐闭合。电化学测试结果表明, 与 MAO 陶瓷层和 LDH/MAO 涂层相比, 超疏水 LDH/MAO 复合涂层具有最低的腐蚀电流密度、最正的腐蚀电位以及最大的阻抗模量; 浸泡实验结果证明, 具有主动防护性能的超疏水 LDH/MAO 涂层可以显著提高 MAO 陶瓷层的长期耐蚀性能。

关键词: 镁合金; 微弧氧化; 层状双金属氢氧化物; 超疏水性; 耐蚀性

(Edited by Bing YANG)